*Geochemistry International, Vol. 39, No. 9, 2001, pp. 831–847. Translated from Geokhimiya, No. 9, 2001, pp. 915–932.*


# The Structure of the Layered Complex of the Voikar Ophiolite Association (Polar Urals) as an Indicator of Mantle Processes beneath a Back-Arc Sea

**E. V. Sharkov, A. V. Chistyakov, and E. E. Laz'ko**

*Institute of Geology of Ore Deposits, Petrography, Mineralogy, and Geochemistry, Russian Academy of Sciences, Staromonetnyi per. 35, Moscow, 109017 Russia*

Received January 31, 2001

**Abstract**—The vertical cross section and evolution of the major mineral phases were studied in the Layered complex of the Late Devonian Voikar ophiolite association. The complex consists of two megarhythms separated by a transitional zone. The megarhythms are similar in structure and are characterized by a gradation from ultrabasic rocks at the bottom to gabbroids at the top. The Upper megarhythm differs from the Lower one owing to the occurrence of orthopyroxene in the gabbroids. The Transitional zone between the megarhythms has the reverse sequence (grading upsection from basic to ultrabasic rocks). Based on this study and previous isotopic data [1, 2], we concluded that the parental magmas of the Lower megarhythm were derived from a slightly depleted mantle source, similarly to rocks of the ultrabasic complex of this association. The magmas of the Upper megarhythm were derived from a more depleted mantle and were contributed by an ancient material from a subducted plate or mixed with subduction-related magmas. We suggest that the Layered complex represents a well-preserved fragment of the lower crust in the back-arc setting. This crustal domain originated from intrusions of newly formed magmas along the crust–mantle boundary. The formation of the lower crust was accompanied by the spreading of the mantle plume head, which resulted in the shearing of mantle peridotites and the overlying newly formed hot cumulates. In terms of geodynamics, the first stage of the formation of the Voikar ophiolites was related to the opening of a back-arc basin, while the second stage reflected the initiation and evolution of a subduction zone.

## INTRODUCTION

Most researchers now believe that the layered (gabbroid) complexes of ophiolite associations are former shallow chambers accumulating magmas emplaced from beneath the zones of oceanic and back-arc spreading [3–6]. The complexes show explicit layering generally with upsection gradation from ultrabasic to basic rocks and are similar in this respect to the large continental layered mafic–ultramafic intrusions. This suggests that analogous petrogenetic processes can operate within both the oceanic and continental crusts. Detailed studies of rock sequences and variation of mineral compositions over the sections of ophiolite complexes and large continental layered intrusions can help in modeling processes that control the evolution of such important magmatic systems. We studied the well-preserved layered complex of the Paleozoic Voikar ophiolite massif in the Polar Urals. Our aim was to determine the structure of the layered complex, the evolution of its mineral composition, and its relation to processes in the upper mantle during the formation of a structure with an oceanic-type lithosphere and the emplacement of the Voikar ophiolite massif as a fragment of this structure.

## GEOLOGY OF THE VOIKAR OPHIOLITE MASSIF

The Ural Mountains are generally composed of Paleozoic rock complexes between the Russian craton in the west and the Siberian block in the east. The Uralian Ocean was closed after the Late Permian collision of these continents, when the pelagic sediments, oceanic lithosphere, and island-arc complexes were moved westward and thrust over the shelf sediments of the ancient passive continental margin of the Russian craton [7, 8]. The tectonic fragments of the oceanic lithosphere and island-arc complexes are almost continuously exposed along the eastern slope of the Urals and form an ophiolite zone up to 250 km wide and more than 2000 km long.

The Main Ural Fault, the major tectonic element of the region, is an extensive zone of shearing and serpentinite melange about 20 km wide and is traced along the whole mountain range. This fault was responsible for thrusting ophiolitic and island-arc rocks over the ancient continental margin. The well-preserved ophiolite massifs near the Main Ural Fault form nappes or large blocks among the serpentinite melange.

The Voikar–Syn'inskii massif in the Polar Urals is one of these massifs, which is traced from north to

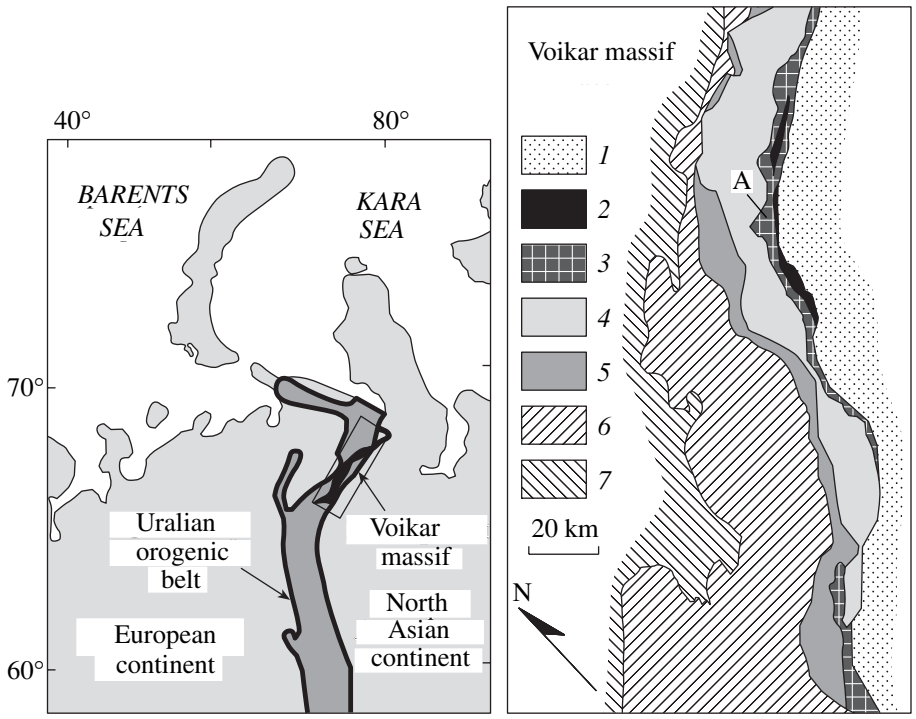


**Fig. 1.** Schematic map of the Voikar massif. (*1*) Diorites, tonalites, and island-arc volcanics of the Lagorta sheet; (*2, 3*) Voikar ophiolites: (*2*) parallel dike complex, (*3*) gabbros and cumulative ultramafic rocks; (*4*) mantle peridotites; (*5*) metamorphozed gabbro, plagiogranites and marbles of the Khulga sheet; (*6*) pelagic and volcano-sedimentary rocks; (*7*) shelf deposits. A denotes section location.

south for about 200 km and has a width of up to 20 km [3, 9, 10]. It consists of three southeast-dipping sheets separated by detachment faults (Fig. 1), which compose a typical stratified ophiolite association. The lower Khulga sheet, up to 4 km thick, consists of intensely deformed and metamorphozed gabbros, plagiogranites, and marbles. The metamorphosed basic rocks are transformed into chlorite–lawsonite, glaucophane, and garnet–glaucophane schists with phengite and chrome melanite, or into zoisite and garnet amphibolites, which are locally migmatized and include numerous plagiogranite veins. The middle Paier sheet, 1–9 km thick, comprises peridotites, pyroxenites, gabbros, and diabases of the Voikar ophiolite massif. The upper Lagorta sheet, >1.5 km thick, generally consists of quartz diorites and tonalites.

The section of the Paier sheet begins with ultrabasic mantle rocks. The ultrabasic complex is overlain by a zone of homogeneous (marginal) dunites, which grade upward to rhythmically layered ultramafites and gabbroids. In tectonically undeformed sections, the ultrabasic rocks of the gabbroid complex also underlay peridotites. The transition between the ultrabasic and gabbroic complexes normally does not show a distinct unconformity and is represented by a zone with alternated lens-shaped bodies of tectonized peridotites and marginal dunites. The amount of peridotite bodies in this zone gradually decreases upward. The transition zone is locally complicated by tectonic displacements.

The structure of the layered complex has been studied less than the complex of mantle ultrabasites, which were characterized in a series of publications [1, 3, 9]. We studied the layered complex in the northern part of the Voikar massif along the Truba-Yu River. A schematic map of the area is given in Fig. 2, while a generalized section across the massif studied by E.E. Laz'ko is shown in Fig. 3.

The layered complex consists of two complicated megarhythms (Fig. 4). The Lower megarhythm begins with a thick (about 500 m) horizon of homogeneous marginal dunites. These are overlain by a horizon with an alternation of dunites, wehrlites, olivine clinopyroxenites, and clinopyroxenites. The horizon is about 2 km in total thickness, more than a half of which is comprised of dunites. The upper part of the horizon includes gabbro interbeds and is overlain by a zone of homogeneous gabbro about 600 m thick with clinopyroxenite interbeds in the uppermost part of the megarhythm. Orthopyroxene in the rocks of the Lower megarhythm occurs only as exsolution lamellae in augite.

The two megarhythms are separated by a Transition zone about 500 m thick composed of alternating dunite and wehrlite layers.

The Upper megarhythm begins with a dunite horizon about 300 m thick with crosscutting veins of oliv-

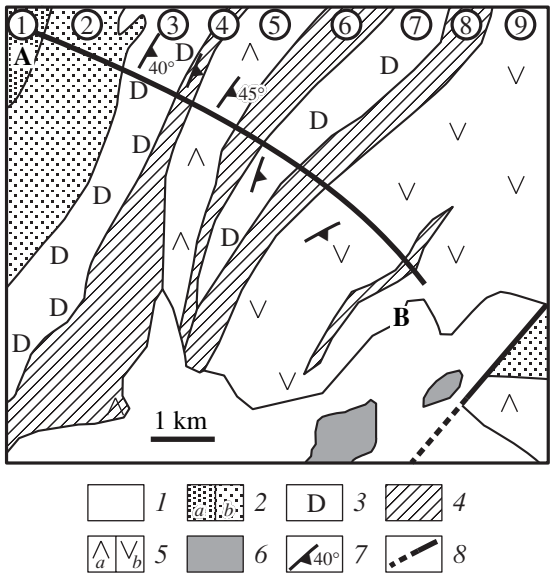


**Fig. 2.** Schematic map of the study area [modified after Efimov *et al*. (1978)].

(*1*) Quaternary deposits; (*2*) mantle harzburgites: *a*, poorly altered and *b*, strongly altered; (*3*) dunites; (*4*) horizons of basic and ultrabasic rock intercalation; (*5*) gabbroids: *a*, gabbro and *b*, gabbronorites; (*6*) diabases from the parallel dike complex; (*7*) layering attitude; (*8*) tectonic sheet boundaries. **A–B** is section location. Numbers in circles: (1, 2) mantle harzburgites (1, moderately altered and 2, strongly altered); (3–5) Lower megarhythm (3, marginal dunites, 4, intercalation horizons, and 5, gabbros); (6) Transitional zone; (7–9) Upper megarhythm (7, dunites, 8, intercalation horizon, and 9, gabbronorites).

ine gabbronorite in its lower part. As in the Lower megarhythm, the dunite horizon is overlain by a zone of alternating wehrlites, clinopyroxenites, gabbro, and gabbronorites (including olivine gabbronorite) about 600 m thick. The proportion of gabbroic rocks increases upsection. The rocks are strongly sheared, but rhythmic layering is locally preserved. The section studied ends with a horizon of gabbronorites and olivine gabbronorites >1000 m thick with a thin dunite horizon at its base.

The detailed Sm–Nd isotopic study dates the rocks of the massif at 387 ± 34 Ma with $\varepsilon Nd(T) = +9.6 \pm 1.8$ and indicates that the rocks of the oceanic crust and mantle harzburgites are complementary and were derived from a single MORB-type source [2]. According to major-element contents and low REE concentrations, the Voikar harzburgites could have originated from the progressive extraction of magma from a nondepleted mantle protolith, and the melt would have begun to separate within the stability field of garnet lherzolite.

## ANALYTICAL TECHNIQUE

The less altered rock samples were collected systematically across the section with an interval of 50–100 m. The horizons with rhythmic layering were sampled more frequently. The mineral compositions (1200 phases) were analyzed with a JEOL 8900 microprobe at the United States Geological Survey, Denver, Colorado. The representative analyses are given in Tables 1–7 and shown in Figs. 5–8.

## PETROGRAPHY

The layered complex of the Voikar ophiolite massif is a large layered intrusion, a former transitional chamber, where the magmas emplaced from beneath the zones of oceanic (or back-arc) spreading accumulated and crystallized. However, in contrast to the rocks of the continental layered intrusions that were emplaced into the rigid framework and preserve primary magmatic structures and textures, the rocks of the ophiolite complexes underwent extensive high-temperature blastic mylonitisation. Actually, they represent the metamorphosed magmatic rocks, and cumulative textures are rare in them. Nevertheless, we described these rocks in terms of magmatism. The metamorphic alteration occurred under greenschist-facies conditions and resulted in the serpentinization of ultramafic rocks and the amphibolization of gabbroids with the extensive development of fibrous amphibole of the tremolite–actinolite series after pyroxenes and the formation of sau-

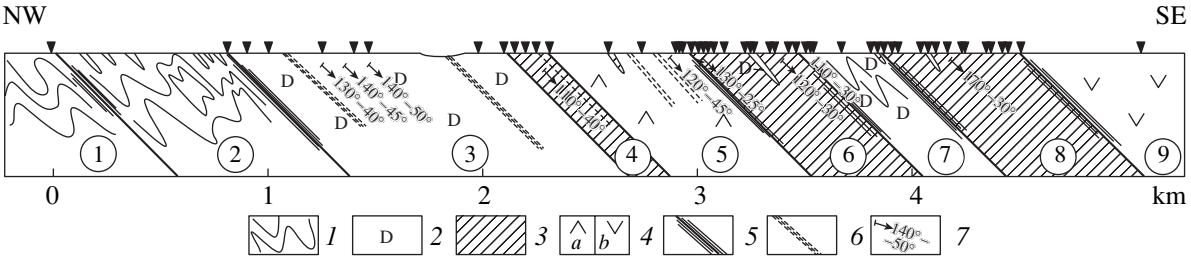


**Fig. 3.** Geological section across the Layered complex.

(*1*) Mantle harzburgites; (*2*) dunites; (*3*) horizons of basic and ultrabasic rock intercalation; (*4*) gabbroids: *a*, gabbro and *b*, gabbronorites; (*5*) unit boundaries; (*6*) thrusts; (*7*) layering dip. Black triangles denote sampling sites. Numbers in circles as in Fig. 2.

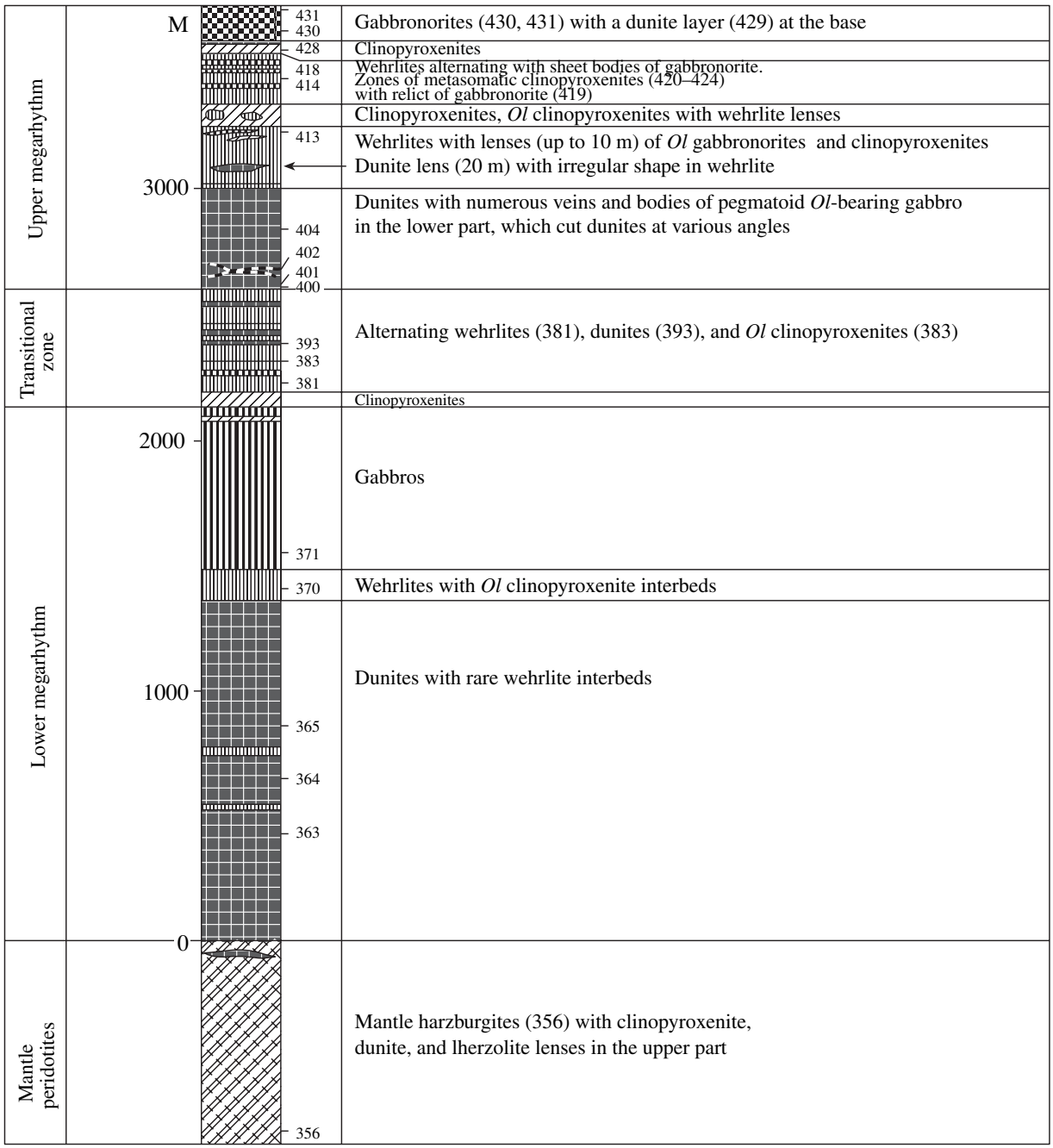


**Fig. 4.** A stratigraphic section across the layered complex of the Voikar ophiolite association. Sampling location and sample numbers (Tables 1–7) are shown.

ssurite and chlorite (with accessory clinozoisite) after plagioclase.

**Mantle peridotites (harzburgites).** The mantle peridotites have protogranular (up to porphyroclastic) textures similar to those described by A. Nicolas [4]. The main minerals are 70–80 vol % olivine (*Ol*) $Fo_{90–91}$, 20–30 vol % orthopyroxene (*Opx*) $W_1En_{90}Fs_9$, 1–7 vol % clinopyroxene (*Cpx*) $W_{50–51}En_{45–47}Fs_{3–4}$, and <1–2% chrome spinel (*CrSp*); pale green edenite-like amphibole compose <1%. Large olivine and orthopyroxene grains in samples with a protogranular texture are subhedral or anhedral and normally show evidence of deformation (undulatory mosaic extinction and deformation twinning). Numerous exsolution lamellae of clinopyroxene are typical of the inner parts of the large orthopyroxene crystals. Clinopyroxene normally occurs in interstices between olivine and orthopyroxene grains. Small

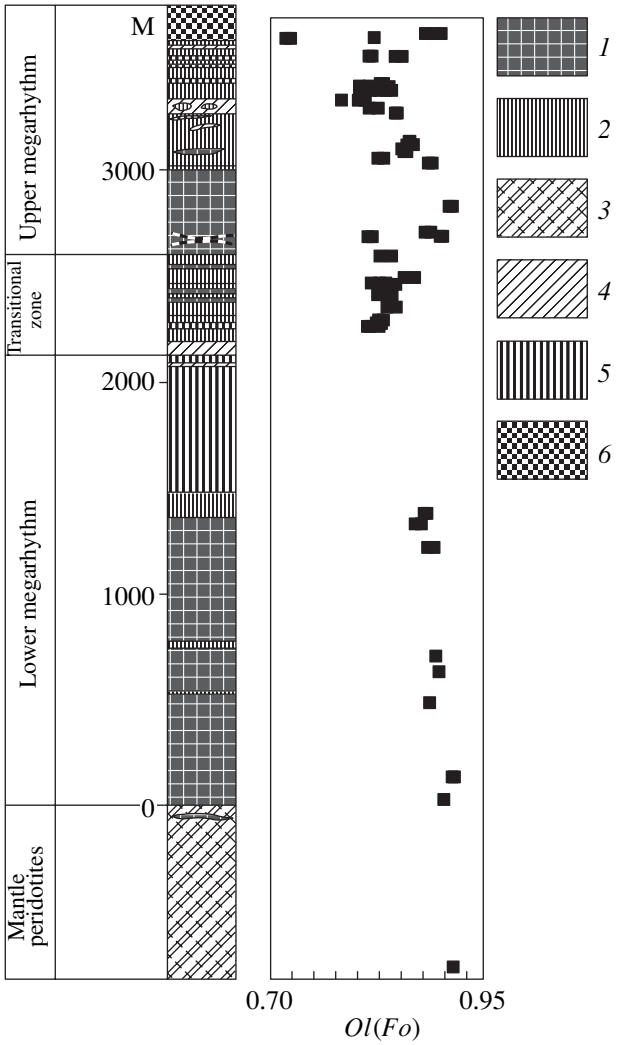


**Fig. 5.** Variation of olivine composition over the section. (*1*) Dunite, (*2*) wehrlite, (*3*) harzburgite, (*4*) clinopyroxenite, (*5*) gabbro and gabbronorites, (*6*) upper gabbronorite.

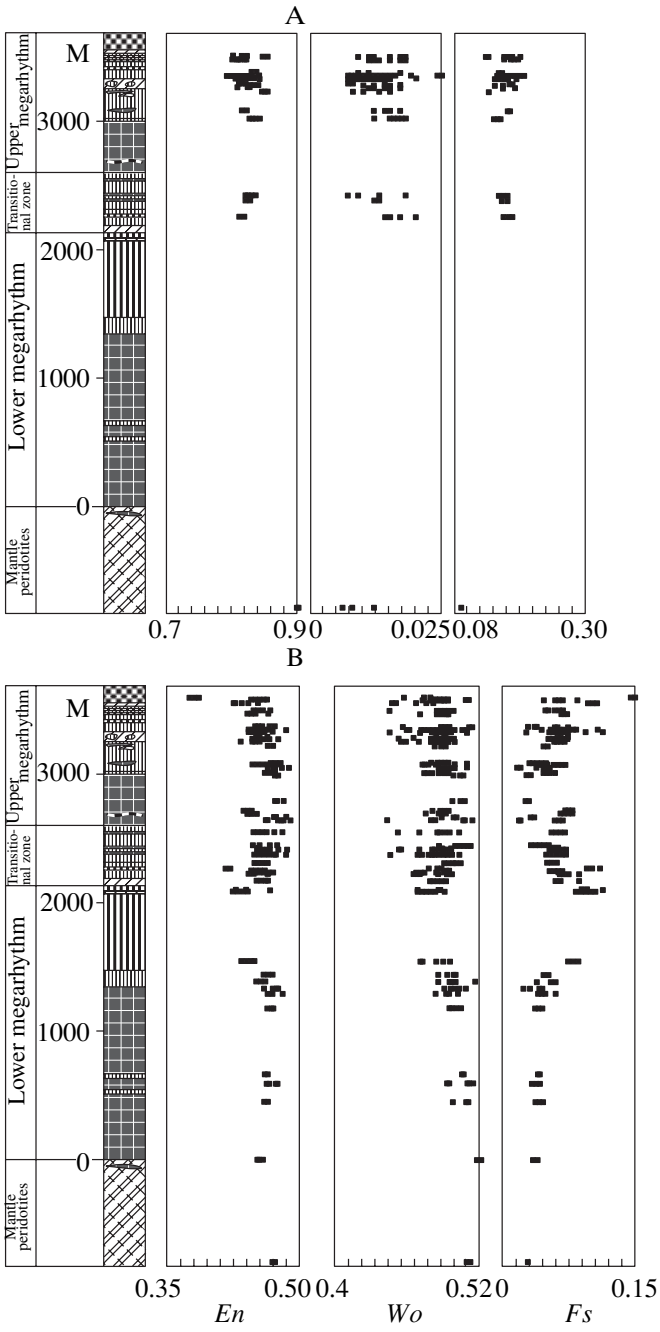


**Fig. 6.** Variation of pyroxene composition over the section. (A) Orthopyroxene, (B) clinopyroxene. See Fig. 5 for symbol explanation.

pyroxene grains are usually devoid of clinopyroxene lamellae and are associated with edenite-type amphibole replacing clinopyroxene. Semitransparent red-brown spinel forms subhedral or curved vermicular grains and contains 23.0–25.6 wt % $Cr_2O_3$ and 41.7–43.3 wt % $Al_2O_3$ in the studied sample.

Olivine and orthopyroxene in the cataclastic rock samples compose elongated deformed porphyroclasts. Their grains do not exceed 5–6 mm in size. Deformations in minerals are pronounced in undulatory mosaic extinction and kink bands in olivine and lamella curvature in orthopyroxene. Neoblastic assemblage consists of *Ol*, *Opx, Cpx*, and *Sp*. Olivine and orthopyroxene neoblasts are small polygonal grains, which normally show no deformation features and are located along the porphyroblast margins or are traced across them as grain chains. *Cpx* neoblasts occur as irregularly shaped interstitial grains, while spinel forms lens-shaped and vermicular aggregates and grains.

**Dunites** are coarse- to medium-grained rocks composed of olivine with about 2–5 vol % of anhedral chrome spinel and diopside grains. Regardless of the location in the section of the layered complex, the olivine composition in dunites is rather uniform and corresponds to $Fo_{88–91}$. Clinopyroxene (diopside, $W_{48–50}En_{46–48}Fs_{2–6}$) occurs in small amounts in the interstices of olivine grains.

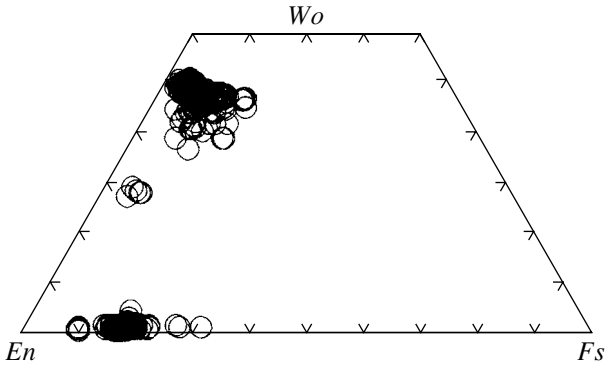


**Fig. 7.** Compositions of the studied pyroxenes.

Chrome spinel is present in the interstices of grains and as inclusions in olivine and clinopyroxene. Unlike the olivine and clinopyroxene, the chrome spinel composition in metadunites is related to the rock location in the section. For example, spinel in the lower megarhythm is moderately chromian (29.7–35.1 wt % $Cr_2O_3$) and relatively highly aluminous (20.7–29.8 wt % $Al_2O_3$). The cross-section variation in the spinel composition is not very regular; however, the Al contents slightly increase upsection, while Cr and Fe contents slightly decrease. Spinel in the dunite horizon of the upper megarhythm is more chromian with increasing $Cr_2O_3$ contents from 40.4 to 52.8 wt % and decreasing $Al_2O_3$ contents from 20.1 to 7.9 wt % downsection to the megarhythm base at almost constant Fe contents. The reverse compositional variations are typical only of the Transitional zone, where Al and Fe contents decrease upsection, while Cr contents increase.

During the low-temperature alteration, olivine is replaced extensively by reticular chrysotile-type serpentine and only locally preserved as relicts; chrome spinel is rimmed by magnetite.

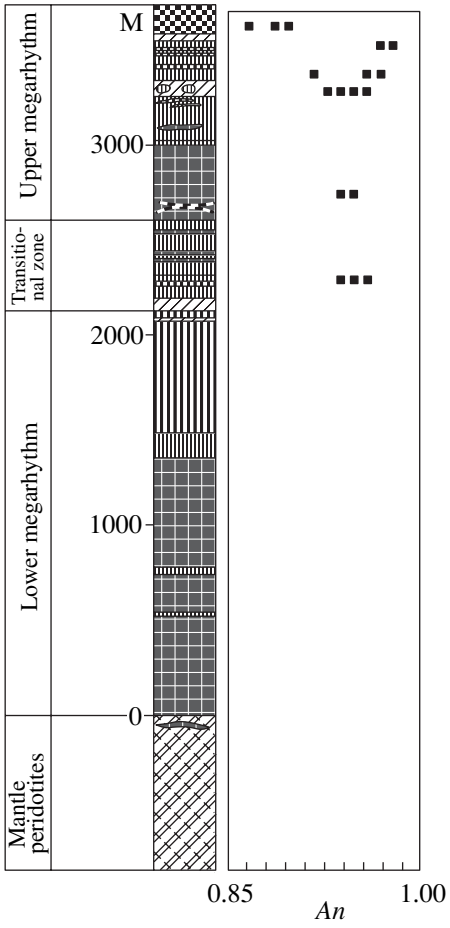


**Fig. 8.** Variation of plagioclase composition over the section. See Fig. 5 for symbol explanation.

**Wehrlites and olivine clinopyroxenites** differ only in olivine proportions (30–40 and 10–20 vol %, respectively). Clinopyroxene porphyroclasts usually form elongated grains (in places, nearly euhedral) 3–8 mm in length with slightly rounded edges. Some clinopyrox-

**Table 1.** Representative analyses of olivine from the rocks of the Voikar ophiolite complex (wt %)

| Sample | 356 | 363 | 364 | 393 | 400 | 404 | 405 | 429 | 381 | 383 | 418 | 423 | 402 | 413 |
|---|---|---|---|---|---|---|---|---|---|---|---|---|---|---|
| $SiO_2$ | 41.17 | 40.58 | 41.61 | 40.60 | 40.87 | 41.21 | 40.86 | 40.75 | 38.93 | 40.58 | 40.52 | 40.46 | 39.64 | 38.50 |
| FeO | 8.60 | 11.17 | 10.41 | 12.24 | 9.39 | 8.42 | 10.87 | 10.33 | 17.05 | 16.08 | 15.27 | 16.35 | 19.83 | 25.6 |
| MnO | 0.13 | 0.17 | 0.16 | 0.22 | 0.19 | 0.12 | 0.19 | 0.28 | 0.26 | 0.23 | 0.26 | 0.21 | 0.35 | 0.32 |
| MgO | 49.57 | 47.84 | 48.84 | 46.27 | 48.88 | 50.42 | 48.63 | 47.97 | 43.18 | 44.32 | 44.72 | 44.23 | 40.67 | 36.77 |
| CaO | 0.00 | 0.02 | 0.06 | 0.02 | 0.02 | 0.04 | 0.01 | 0.01 | 0.03 | 0.02 | 0.03 | 0.03 | 0.00 | 0.01 |
| NiO | 0.45 | 0.25 | 0.28 | 0.26 | 0.16 | 0.13 | 0.24 | 0.26 | 0.06 | 0.09 | 0.13 | 0.14 | 0.07 | 0.10 |
| Total | 99.92 | 100.03 | 101.39 | 99.67 | 99.55 | 100.38 | 100.84 | 99.61 | 99.54 | 101.34 | 100.97 | 101.45 | 100.60 | 101.33 |
| *Fo* | 0.91 | 0.88 | 0.89 | 0.87 | 0.90 | 0.91 | 0.89 | 0.89 | 0.82 | 0.83 | 0.84 | 0.83 | 0.79 | 0.72 |

Note: 356—mantle peridotites (harzburgites). Rock of the layered series: (Lower megarhythm) 363–365—dunites; 370—wehrlites; 371—gabbro; (Transitional zone) 381—wehrlite; 383 and 388—olivine clinopyroxenites; 393—dunite; (Upper megarhythm) 400, 401, 404, 405, and 429—dunites; 402, 413, and 423—olivine gabbronorites; 418, 424, and 427—wehrlites; 419, 430, and 431—gabbronorites; 420 and 421—metasomatic clinopyroxenites; 423 and 428a—olivine clinopyroxenites; 428—clinopyroxenites.

**Table 2.** Representative analyses of clinopyroxene from the rocks of the Voikar ophiolite complex (wt %)

| Sample | 356 | 363 | 364 | 370 | 371 | 381 | 381 | 383 | 388 | 388 | 393 | 402 | 404 |
|---|---|---|---|---|---|---|---|---|---|---|---|---|---|
| $SiO_2$ | 53.18 | 52.85 | 53.81 | 53.05 | 52.55 | 53.24 | 52.68 | 53.10 | 53.85 | 53.79 | 54.34 | 53.18 | 54.33 |
| $TiO_2$ | 0.14 | 0.29 | 0.29 | 0.15 | 0.24 | 0.07 | 0.13 | 0.09 | 0.12 | 0.08 | 0.09 | 0.18 | 0.06 |
| $Al_2O_3$ | 2.89 | 2.49 | 2.50 | 2.59 | 2.78 | 2.15 | 2.83 | 2.95 | 2.46 | 2.84 | 1.23 | 2.53 | 1.40 |
| $Cr_2O_3$ | 0.70 | 0.52 | 0.68 | 0.69 | 0.12 | 0.16 | 0.36 | 0.70 | 0.53 | 0.66 | 0.31 | 0.12 | 0.68 |
| FeO | 1.77 | 2.84 | 2.48 | 3.28 | 5.38 | 4.08 | 4.43 | 3.96 | 3.93 | 4.54 | 2.48 | 4.51 | 1.83 |
| MnO | 0.08 | 0.09 | 0.10 | 0.12 | 0.18 | 0.14 | 0.14 | 0.15 | 0.12 | 0.10 | 0.09 | 0.17 | 0.09 |
| MgO | 16.53 | 16.33 | 16.73 | 16.41 | 15.66 | 15.88 | 16.34 | 15.93 | 16.09 | 17.21 | 16.61 | 15.72 | 17.18 |
| CaO | 24.27 | 23.87 | 23.76 | 23.90 | 22.61 | 23.91 | 22.62 | 23.81 | 23.44 | 21.74 | 24.42 | 23.30 | 24.16 |
| $Na_2O$ | 0.16 | 0.21 | 0.30 | 0.22 | 0.24 | 0.04 | 0.10 | 0.09 | 0.13 | 0.11 | 0.10 | 0.16 | 0.27 |
| $K_2O$ | 0.02 | 0.02 | 0.02 | 0.02 | 0.03 | 0.02 | 0.01 | 0.00 | 0.02 | 0.03 | 0.01 | 0.02 | 0.03 |
| NiO | 0.07 | 0.05 | 0.04 | 0.02 | 0.01 | 0.07 | 0.07 | 0.01 | 0.00 | 0.00 | 0.03 | 0.03 | 0.00 |
| Total | 99.81 | 99.56 | 100.71 | 100.45 | 99.80 | 99.76 | 99.71 | 100.79 | 100.69 | 101.10 | 99.71 | 99.92 | 100.03 |
| *En* | 0.47 | 0.47 | 0.47 | 0.46 | 0.45 | 0.45 | 0.47 | 0.45 | 0.46 | 0.49 | 0.47 | 0.45 | 0.48 |
| *Wo* | 0.50 | 0.49 | 0.49 | 0.49 | 0.47 | 0.49 | 0.46 | 0.49 | 0.48 | 0.44 | 0.49 | 0.48 | 0.49 |
| *Fs* | 0.03 | 0.05 | 0.04 | 0.05 | 0.09 | 0.06 | 0.07 | 0.06 | 0.06 | 0.07 | 0.04 | 0.07 | 0.03 |
| Sample | 413 | 413 | 418 | 419 | 420 | 421 | 423 | 424 | 424 | 424 | 428a | 430 | 431 |
| $SiO_2$ | 51.21 | 51.98 | 52.86 | 53.19 | 52.45 | 53.37 | 53.40 | 54.19 | 57.70 | 53.18 | 54.85 | 52.29 | 51.70 |
| $TiO_2$ | 0.31 | 0.26 | 0.17 | 0.08 | 0.14 | 0.14 | 0.09 | 0.07 | 0.03 | 0.16 | 0.00 | 0.35 | 0.30 |
| $Al_2O_3$ | 3.52 | 3.33 | 3.20 | 2.33 | 2.67 | 2.92 | 2.67 | 1.65 | 2.06 | 3.27 | 0.08 | 2.57 | 2.76 |
| $Cr_2O_3$ | 0.01 | 0.02 | 0.71 | 0.35 | 0.25 | 0.40 | 0.50 | 0.31 | 0.28 | 0.57 | 0.21 | 0.02 | 0.00 |
| FeO | 7.13 | 8.99 | 4.09 | 4.68 | 4.70 | 4.60 | 4.09 | 3.74 | 2.66 | 5.32 | 3.16 | 9.16 | 7.05 |
| MnO | 0.15 | 0.21 | 0.10 | 0.11 | 0.14 | 0.12 | 0.13 | 0.10 | 0.10 | 0.11 | 0.11 | 0.27 | 0.20 |
| MgO | 14.26 | 15.10 | 15.99 | 16.21 | 16.09 | 15.87 | 15.97 | 16.62 | 22.79 | 17.85 | 16.45 | 12.91 | 14.32 |
| CaO | 23.31 | 20.2 | 22.96 | 23.12 | 23.3 | 23.3 | 23.55 | 24.25 | 12.80 | 20.13 | 25.17 | 22.52 | 22.84 |
| $Na_2O$ | 0.18 | 0.20 | 0.16 | 0.17 | 0.15 | 0.12 | 0.13 | 0.05 | 0.47 | 0.12 | 0.04 | 0.22 | 0.23 |
| $K_2O$ | 0.02 | 0.03 | 0.02 | 0.03 | 0.02 | 0.03 | 0.01 | 0.02 | 0.04 | 0.03 | 0.02 | 0.00 | 0.02 |
| NiO | 0.00 | 0.02 | 0.01 | 0.02 | 0.03 | 0.00 | 0.04 | 0.00 | 0.00 | 0.05 | 0.05 | 0.00 | 0.05 |
| Total | 100.10 | 100.30 | 100.27 | 100.29 | 99.94 | 100.87 | 100.58 | 101.00 | 98.93 | 100.79 | 100.14 | 100.31 | 99.47 |
| *En* | 0.41 | 0.44 | 0.46 | 0.46 | 0.45 | 0.45 | 0.45 | 0.46 | 0.68 | 0.51 | 0.45 | 0.38 | 0.41 |
| *Wo* | 0.48 | 0.42 | 0.47 | 0.47 | 0.47 | 0.48 | 0.48 | 0.48 | 0.28 | 0.41 | 0.50 | 0.47 | 0.47 |
| *Fs* | 0.11 | 0.15 | 0.07 | 0.07 | 0.07 | 0.07 | 0.07 | 0.06 | 0.04 | 0.08 | 0.05 | 0.15 | 0.11 |

ene grains include orthopyroxene lamellae, which are normally replaced by irregular grains of pale green amphibole. Rare orthopyroxene grains locally occur in wehrlites and clinopyroxenites in the upper parts of the megarhythms. Olivine usually has complicated forms, but in places appears as rounded grains. Relict textures indicate that both porphyroclasts and neoblasts of olivine are present in the rocks. Irregularly shaped grains of chrome spinel also occur in the rocks in small amounts. As in dunites, the chrome spinel composition depends on the host mineral. Plagioclase is occasionally present in interstices and is normally replaced by chlorite.

Olivine in wehrlites and clinopyroxenites is compositionally uniform over the cross section of the layered complex and corresponds to $Fo_{82–84}$. The clinopyroxene composition in these rocks is also reasonably uniform and is $W_{48–51}En_{45–46}Fs_{4–6}$ in the lower megarhythm and $W_{42–50}En_{43–47}Fs_{3–7}$ in the upper megarhythm. The orthopyroxene composition is $W_{1–2}En_{81–85}Fs_{13–15}$ in the rocks of the upper megarhythm and is slightly more ferrous ($W_{1–2}En_{81–84}Fs_{16–18}$) in wehrlites of the transitional zone. Rare interstitial plagioclase grains correspond to $An_{97–98}$.

**Table 3.** Representative analyses of orthopyroxene from the rocks of the Voikar ophiolite complex (wt %)

| Sample | 356 | 383 | 388 | 391 | 402 | 403 | 406 | 409 |
|---|---|---|---|---|---|---|---|---|
| $SiO_2$ | 55.98 | 55.20 | 55.40 | 55.33 | 55.41 | 54.72 | 56.30 | 55.69 |
| $TiO_2$ | 0.04 | 0.06 | 0.04 | 0.03 | 0.07 | 0.08 | 0.03 | 0.10 |
| $Al_2O_3$ | 3.34 | 2.87 | 3.29 | 2.45 | 1.96 | 2.24 | 1.08 | 2.05 |
| $Cr_2O_3$ | 0.59 | 0.42 | 0.49 | 0.37 | 0.04 | 0.04 | 0.36 | 0.42 |
| FeO | 5.96 | 10.84 | 10.89 | 10.53 | 12.05 | 13.42 | 10.15 | 10.99 |
| MnO | 0.12 | 0.23 | 0.24 | 0.25 | 0.32 | 0.33 | 0.29 | 0.26 |
| MgO | 33.76 | 30.29 | 29.98 | 30.91 | 29.54 | 28.27 | 31.07 | 30.07 |
| CaO | 0.60 | 0.87 | 0.61 | 0.48 | 0.73 | 0.78 | 0.79 | 0.76 |
| NiO | 0.07 | 0.01 | 0.07 | 0.00 | 0.01 | 0.01 | 0.05 | 0.06 |
| Total | 100.46 | 100.79 | 101.01 | 100.35 | 100.13 | 99.89 | 100.12 | 100.40 |
| *En* | 0.90 | 0.82 | 0.82 | 0.83 | 0.80 | 0.78 | 0.83 | 0.82 |
| *Wo* | 0.01 | 0.02 | 0.01 | 0.01 | 0.02 | 0.02 | 0.02 | 0.01 |
| *Fs* | 0.09 | 0.16 | 0.17 | 0.16 | 0.18 | 0.20 | 0.15 | 0.17 |

| Sample | 412 | 413 | 418 | 419 | 420 | 421 | 423 | 427 | 433 |
|---|---|---|---|---|---|---|---|---|---|
| $SiO_2$ | 56.32 | 54.18 | 55.72 | 55.20 | 55.53 | 55.52 | 55.98 | 54.87 | 54.85 |
| $TiO_2$ | 0.03 | 0.06 | 0.07 | 0.05 | 0.00 | 0.02 | 0.03 | 0.05 | 0.04 |
| $Al_2O_3$ | 1.57 | 2.14 | 2.45 | 1.87 | 1.92 | 2.44 | 2.48 | 2.22 | 2.34 |
| $Cr_2O_3$ | 0.33 | 0.01 | 0.44 | 0.22 | 0.16 | 0.40 | 0.33 | 0.33 | 0.30 |
| FeO | 9.23 | 16.93 | 9.89 | 12.06 | 11.72 | 12.00 | 10.91 | 10.97 | 12.05 |
| MnO | 0.21 | 0.33 | 0.24 | 0.26 | 0.31 | 0.32 | 0.23 | 0.22 | 0.32 |
| MgO | 31.52 | 26.18 | 30.68 | 29.65 | 30.01 | 29.44 | 30.46 | 30.39 | 29.25 |
| CaO | 0.69 | 0.74 | 0.66 | 0.67 | 0.58 | 0.63 | 0.61 | 0.64 | 0.78 |
| NiO | 0.06 | 0.00 | 0.06 | 0.04 | 0.02 | 0.00 | 0.02 | 0.06 | 0.00 |
| Total | 99.96 | 100.57 | 100.21 | 100.02 | 100.25 | 100.77 | 101.05 | 99.75 | 99.93 |
| *En* | 0.85 | 0.73 | 0.84 | 0.80 | 0.81 | 0.81 | 0.82 | 0.82 | 0.80 |
| *Wo* | 0.01 | 0.01 | 0.01 | 0.02 | 0.01 | 0.01 | 0.01 | 0.01 | 0.02 |
| *Fs* | 0.14 | 0.26 | 0.15 | 0.18 | 0.18 | 0.18 | 0.17 | 0.17 | 0.18 |

**Table 4.** Representative analyses of plagioclase from the rocks of the Voikar ophiolite complex (wt %)

| Sample | 384 | 403 | 413 | 413 | 419 | 419 | 420 | 420 | 427 | 427 | 427 | 430 | 430 |
|---|---|---|---|---|---|---|---|---|---|---|---|---|---|
| $SiO_2$ | 44.78 | 44.58 | 44.5 | 44.94 | 44.97 | 44.56 | 44.47 | 44.51 | 44.84 | 42.91 | 44.51 | 46.23 | 45.98 |
| $Al_2O_3$ | 35.44 | 35.12 | 35.57 | 35.10 | 34.69 | 35.44 | 35.06 | 35.58 | 35.26 | 35.81 | 35.12 | 33.97 | 34.45 |
| FeO | 0.19 | 0.19 | 0.20 | 0.48 | 0.20 | 0.16 | 0.23 | 0.08 | 0.23 | 0.27 | 0.25 | 0.10 | 0.26 |
| CaO | 19.03 | 19.28 | 19.36 | 18.98 | 18.44 | 19.16 | 19.45 | 19.55 | 19.69 | 20.26 | 19.64 | 18.07 | 18.19 |
| $Na_2O$ | 0.59 | 0.58 | 0.48 | 0.76 | 0.87 | 0.43 | 0.44 | 0.34 | 0.35 | 0.18 | 0.31 | 1.20 | 1.11 |
| $K_2O$ | 0.02 | 0.03 | 0.02 | 0.02 | 0.03 | 0.03 | 0.02 | 0.02 | 0.02 | 0.01 | 0.03 | 0.02 | 0.03 |
| Total | 100.05 | 99.78 | 100.13 | 100.28 | 99.16 | 99.78 | 99.67 | 100.08 | 100.39 | 99.44 | 99.86 | 99.59 | 100.02 |
| *An* | 0.95 | 0.95 | 0.96 | 0.93 | 0.92 | 0.96 | 0.96 | 0.97 | 0.97 | 0.98 | 0.97 | 0.89 | 0.90 |

**Table 5.** Representative analyses of amphibole from the rocks of the Voikar ophiolite complex (wt %)

| Sample | 356 | 371 | 386 | 393 | 402 | 413 | 418 | 419 | 419 | 420 | 423 | 427 | 428a | 431a |
|---|---|---|---|---|---|---|---|---|---|---|---|---|---|---|
| $SiO_2$ | 50.79 | 45.72 | 51.61 | 52.81 | 46.15 | 46.20 | 46.86 | 48.46 | 49.14 | 46.78 | 47.42 | 49.16 | 51.93 | 45.46 |
| $TiO_2$ | 0.12 | 0.18 | 0.15 | 0.07 | 0.33 | 0.41 | 0.36 | 0.34 | 0.30 | 0.36 | 0.45 | 0.00 | 0.09 | 0.44 |
| $Al_2O_3$ | 2.89 | 12.32 | 2.23 | 2.03 | 11.99 | 12.08 | 11.04 | 9.25 | 9.25 | 10.97 | 11.08 | 10.06 | 2.76 | 11.39 |
| $Cr_2O_3$ | 0.60 | 0.11 | 0.61 | 0.82 | 0.12 | 0.00 | 0.96 | 0.34 | 0.81 | 0.29 | 1.34 | 0.01 | 0.26 | 0.06 |
| FeO | 3.33 | 7.47 | 3.28 | 2.60 | 7.70 | 8.96 | 5.96 | 6.84 | 6.61 | 7.27 | 6.44 | 6.24 | 4.01 | 10.81 |
| MnO | 0.09 | 0.14 | 0.12 | 0.13 | 0.13 | 0.09 | 0.06 | 008 | 0.07 | 0.05 | 0.04 | 0.09 | 0.11 | 0.18 |
| MgO | 16.21 | 15.59 | 16.33 | 16.64 | 16.84 | 15.69 | 17.48 | 17.68 | 17.75 | 17.39 | 17.05 | 17.83 | 16.47 | 13.71 |
| CaO | 22.86 | 12.54 | 24.02 | 23.13 | 12.08 | 12.18 | 12.57 | 12.18 | 12.19 | 12.35 | 12.38 | 12.84 | 22.72 | 11.99 |
| $Na_2O$ | 0.16 | 2.45 | 0.08 | 0.19 | 1.86 | 1.98 | 1.57 | 1.86 | 1.77 | 1.82 | 1.82 | 0.97 | 0.08 | 1.46 |
| $K_2O$ | 0.02 | 0.14 | 0.01 | 0.03 | 0.14 | 0.15 | 0.09 | 0.04 | 0.03 | 0.09 | 0.03 | 0.02 | 0.04 | 0.05 |
| NiO | 0.03 | 0.04 | 0.04 | 0.02 | 0.00 | 0.02 | 0.03 | 0.05 | 0.06 | 0.05 | 0.04 | 0.02 | 0.00 | 0.03 |
| Total | 97.10 | 96.69 | 98.47 | 98.46 | 97.34 | 97.75 | 96.98 | 97.12 | 97.97 | 97.44 | 98.07 | 97.23 | 98.47 | 95.57 |

**Table 6.** Representative analyses of chrome spinel from the rocks of the Voikar ophiolite complex (wt %)

| Sample | 356 | 363 | 364 | 370 | 383 | 388 | 393 | 400 | 404 | 405 | 418 | 423 | 424 | 427 | 429 |
|---|---|---|---|---|---|---|---|---|---|---|---|---|---|---|---|
| $TiO_2$ | 0.07 | 0.52 | 0.42 | 0.16 | 0.12 | 0.15 | 0.16 | 0.26 | 0.19 | 0.21 | 0.24 | 0.33 | 0.30 | 0.26 | 0.17 |
| $Al_2O_3$ | 41.82 | 26.21 | 27.48 | 33.94 | 28.36 | 32.95 | 23.89 | 18.52 | 17.44 | 9.85 | 29.49 | 24.31 | 30.10 | 24.96 | 28.93 |
| $Cr_2O_3$ | 25.60 | 31.15 | 34.73 | 28.13 | 24.63 | 25.29 | 35.88 | 41.92 | 45.24 | 52.56 | 25.43 | 26.87 | 23.12 | 25.18 | 27.9 |
| $Fe_2O_3$ | 2.90 | 11.03 | 6.53 | 6.94 | 14.71 | 9.36 | 7.33 | 7.21 | 7.32 | 7.41 | 12.67 | 16.28 | 14.09 | 17.46 | 10.6 |
| FeO | 11.89 | 20.61 | 17.74 | 19.76 | 25.84 | 21.39 | 22.38 | 22.51 | 16.09 | 23.44 | 23.98 | 23.44 | 24.77 | 23.52 | 19.34 |
| MnO | 0.21 | 0.33 | 0.33 | 0.32 | 0.41 | 0.43 | 0.41 | 0.48 | 0.38 | 0.57 | 0.35 | 0.34 | 0.38 | 0.34 | 0.65 |
| MgO | 17.20 | 10.10 | 11.94 | 11.50 | 6.83 | 9.97 | 8.16 | 7.62 | 11.63 | 6.43 | 8.11 | 7.71 | 7.72 | 7.72 | 10.39 |
| NiO | 0.24 | 0.15 | 0.12 | 0.04 | 0.08 | 0.08 | 0.04 | 0.00 | 0.08 | 0.02 | 0.14 | 0.14 | 0.11 | 0.16 | 0.16 |
| Total | 99.93 | 100.10 | 99.29 | 100.79 | 101.00 | 99.63 | 98.25 | 98.52 | 98.39 | 100.49 | 100.42 | 99.49 | 100.59 | 99.63 | 98.15 |
| Cations for 4 oxygens | | | | | | | | | | | | | | | |
| Al | 1.37 | 0.96 | 0.99 | 1.18 | 1.04 | 1.17 | 0.90 | 0.72 | 0.66 | 0.39 | 1.07 | 0.91 | 1.09 | 0.94 | 1.06 |
| Cr | 0.56 | 0.76 | 0.84 | 0.66 | 0.61 | 0.60 | 0.91 | 1.09 | 1.15 | 1.41 | 0.62 | 0.68 | 0.56 | 0.63 | 0.68 |
| Fe3 | 0.06 | 0.26 | 0.15 | 0.15 | 0.34 | 0.21 | 0.18 | 0.18 | 0.18 | 0.19 | 0.29 | 0.39 | 0.33 | 0.42 | 0.25 |
| Fe2 | 0.28 | 0.53 | 0.45 | 0.49 | 0.67 | 0.54 | 0.60 | 0.62 | 0.43 | 0.66 | 0.62 | 0.63 | 0.64 | 0.63 | 0.50 |
| Mg | 0.71 | 0.47 | 0.54 | 0.51 | 0.32 | 0.45 | 0.39 | 0.37 | 0.56 | 0.32 | 0.37 | 0.37 | 0.36 | 0.37 | 0.45 |

**Table 7.** Representative analyses of magnetite from the rocks of the Voikar ophiolite complex (wt %)

| Sample | 413 | 413 | 413 | 413 | 424 | 428a |
|---|---|---|---|---|---|---|
| $TiO_2$ | 0.53 | 6.21 | 1.15 | 5.15 | 0.72 | 0.68 |
| $Al_2O_3$ | 1.03 | 1.37 | 1.26 | 1.24 | 0.27 | 0.04 |
| $Cr_2O_3$ | 0.19 | 0.20 | 0.16 | 0.22 | 8.68 | 0.00 |
| $Fe_2O_3$ | 66.19 | 55.5 | 65.93 | 58.02 | 59.10 | 67.57 |
| FeO | 31.24 | 36.54 | 32.28 | 35.60 | 30.82 | 31.15 |
| MnO | 0.03 | 0.23 | 0.05 | 0.19 | 0.16 | 0.06 |
| MgO | 0.12 | 0.22 | 0.19 | 0.28 | 0.57 | 0.17 |
| NiO | 0.07 | 0.04 | 0.03 | 0.05 | 0.19 | 0.14 |
| Total | 99.40 | 100.31 | 101.05 | 100.75 | 100.51 | 99.81 |
| Cations for 4 oxygens | | | | | | |
| Ti | 0.02 | 0.18 | 0.03 | 0.15 | 0.02 | 0.02 |
| Al | 0.05 | 0.06 | 0.06 | 0.06 | 0.01 | 0.00 |
| Cr | 0.01 | 0.01 | 0.00 | 0.01 | 0.26 | 0.00 |
| $Fe^{3+}$ | 1.92 | 1.58 | 1.87 | 1.65 | 1.69 | 1.96 |
| $Fe^{2+}$ | 1.01 | 1.16 | 1.02 | 1.12 | 0.98 | 1.00 |
| Mg | 0.01 | 0.01 | 0.01 | 0.02 | 0.03 | 0.01 |

The chrome spinel composition varies insignificantly in wehrlites and clinopyroxenites of the Lower megarhythm. The $Cr_2O_3$ contents range from 28.1 to 29.4 wt % at $Al_2O_3$ contents of 30.4–33.9 wt %. The $Cr_2O_3$ concentration in spinel varies significantly across the Transitional zone from 20.1 wt % at the base and 23 wt % at its top to 30.9 wt % in the middle part of the zone. The $Al_2O_3$ concentrations in spinel range from 27.2 to 35.2 wt %. The spinel composition is more homogeneous within the upper megarhythm. The $Cr_2O_3$ concentration varies from 21.4 to 27 wt % and increases in some grains up to 41.8 and 33.4 wt %, respectively, at the base of the megarhythm and at the boundary of the upper ultrabasic rock layer. The $Al_2O_3$ concentration varies from 24 to 34 wt %. Note that chrome spinel in the same sample is more chromian and less aluminous when occurs in clinopyroxene and more ferric and aluminous when included in olivine.

The neoblastic assemblage consists of clinopyroxene and olivine, which commonly compose small (≤1 mm) polygonal grains along the porphyroclast boundaries or zones crossing the clinopyroxene porphyroclasts. The compositions of the porphyroblastic and neoblastic minerals are almost similar. The low-temperature alteration is normally not extensive and comprises up to 30–50% of the rock volume. Clinopyroxene is weakly replaced by tremolite, while olivine is strongly altered to serpentine. Chrome spinel is rimmed by magnetite, and plagioclase is replaced by chlorite.

**Clinopyroxenites** are also abundant within the layered horizons and are represented there by the following two types: (1) olivine-free clinopyroxenites that are similar in many respects to the olivine clinopyroxenites mentioned above and represent primary cumulates and (2) clinopyroxenites with corrosion textures typical of metasomatic rocks. The latter occur in all layered horizons of the Upper megarhythm and were developed after different rock varieties from pyroxenites to gabbronorites. The latter case can be exemplified by a series of samples (419 to 424) from the Upper layered horizon. They were collected from a concentrically zoned area with gabbronorite in its center, which is replaced outward by clinopyroxenite grading to the ambient wehrlite.

The mineralogical composition of the first type of clinopyroxenites is similar to that of the olivine clinopyroxenites (excluding olivine). The clinopyroxene compositions in these rocks are also similar. In contrast, clinopyroxene in the second type of clinopyroxenites is subcalcic augite and locally up to pigeonite–augite $W_{28–29}En_{66–68}Fs_{5–6}$. Chromite is absent in these rocks and is replaced by magnetite. There are some transitional clinopyroxenite varieties containing clinopyroxenes of both types (sample 424).

These clinopyroxenites have a similar grade of metamorphic alteration: the development of clinopyroxene neoblasts was followed by low-temperature amphibolization with chloritization of accessory interstitial plagioclase $An_{96–97}$.

**Gabbroids** are the most abundant rocks in the layered complex. They participate in the structure of the layered horizons or form thick separate layers. These mesocratic rocks are strongly altered by low-temperature metamorphism and only locally preserve their primary textures and mineralogical composition. The rock texture in these places is similar to granoblastic with abundant triple-grain junctions. The major minerals are ≤1.5 mm in size. Typical cumulative textures are absent. According to the relict mineral assemblages and rare unaltered samples, the following four types of gabbroids can be distinguished: metagabbro, olivine metagabbro, metagabbronorite, and olivine metagabbronorite. The orthopyroxene-bearing rocks occur only in the Upper megarhythm and are absent in the Lower megarhythm.

Plagioclase in the less altered rocks composes slightly elongated unzoned grains with undulatory extinction and occasional pyroxene inclusions. Pyroxene grains are similar in shape to plagioclase and occasionally have small rounded plagioclase and magnetite inclusions. Unlike plagioclase and pyroxenes, olivine grains show complicated forms. They are usually elongated, curved, crooked, and normally have an undulatory mosaic extinction indicating former deformations. Pale green hornblende (<3–5 vol %) forms oikocrysts with rounded pyroxene and olivine chadacrysts. The hornblende was not deformed and probably crystallized at the final stages of the rock blastic mylonitization.

Plagioclase in gabbroids of the Lower megarhythm is completely altered, and its composition has not been determined. Plagioclase in the Upper megarhythm is less altered. The most calcic plagioclase is found in olivine gabbronorites and corresponds to $An_{95–96}$. Its composition varies from $An_{92}$ to $An_{96}$ in the less altered relict gabbronorites. The *An* proportion in plagioclase decreases in gabbronorites up to $An_{89–90}$ in the upper part of this megarhythm. Plagioclases are almost free of potassium.

The ferrosilite component in clinopyroxene generally increases in gabbroids upsection from $W_{42–49}En_{43–47}Fs_{5–11}$ in gabbro of the Lower megarhythm to $W_{45–48}En_{38–47}Fs_{7–16}$ in the lower part of the gabbronorite unit of the Upper megarhythm. The olivine gabbronorite veins from the dunite layer of the Upper megarhythm contain more magnesian *Cpx* ($W_{47–48}En_{44–45}Fs_{7–8}$), while the *Cpx* in gabbronorite sheet bodies located further upsection is slightly more ferrous ($W_{42–48}En_{41–46}Fs_{10–15}$).

Orthopyroxene is absent in gabbro of the Lower megarhythm. Orthopyroxene in olivine gabbronorites of the Upper megarhythm corresponds to $W_{1–2}En_{80–81}Fs_{18–19}$. Orthopyroxene is more ferrous in the gabbronorite sheet bodies ($W_{1–2}En_{69–74}Fs_{25–30}$).

Olivine composition in gabbroids corresponds to $Fo_{79–81}$. It is $Fo_{79–80}$ in olivine gabbronorite veins in

dunites of the Upper megarhythm, $Fo_{71–73}$ in gabbronorite lenses in the middle part of the Upper megarhythm, and $Fo_{81–83}$ in sheet bodies in the uppermost part of the megarhythm. Thin double coronas locally occur around olivine at its boundary with plagioclase and consist of orthopyroxene in the inner zone and of green spinel–clinopyroxene symplectite in the marginal zone. According to experimental data, such coronas could have originated from a subsolidus reaction between magnesian olivine and calcic plagioclase at $T = 1100–900$°C and $P = 8 \pm 2$ kbar [11]. Having proceeded in the rocks already cataclasized, this reaction points to the subsolidus conditions of early cataclasis and indicates a pressure above 6 kbar. This value could hardly correspond to the lithostatic pressure and is probably characteristic of the shearing overpressure.

## EVOLUTION OF MINERAL COMPOSITION IN THE INTRUSION SECTION

**Olivine** composition is generally dependent on the rock composition rather than on its stratigraphic location (Fig. 5). Olivine in dunites corresponds to $Fo_{88–91}$ and is compositionally similar to that in mantle harzburgite. It is $Fo_{82–84}$ in wehrlites and olivine clinopyroxenites and $Fo_{79–81}$ in metagabbroids. Small nonsystematic variations in olivine compositions across the dunite horizons probably indicate that the magmatic chamber was multiply replenished by magmas from the evolving zone of magma generation.

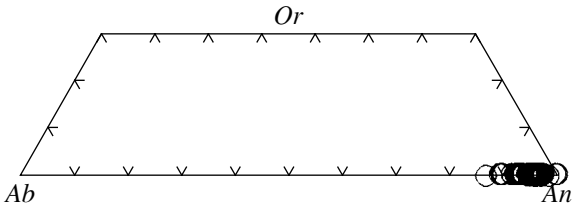


**Fig. 9.** Plagioclase compositions in a *Ab–An–Or* diagram.

**Clinopyroxene** composition also does not depend significantly on the rock stratigraphy (Fig. 6). It corresponds to diopside $W_{48–50}En_{46–48}Fs_{2–6}$ and is close to mantle diopside ($W_{50–51}En_{45–47}Fs_{3–4}$). Clinopyroxene in wehrlites, olivine clinopyroxenites, and clinopyroxenites is $W_{42–50}En_{43–47}Fs_{3–7}$, whereas clinopyroxene in the second (metasomatic) clinopyroxenite type corresponds to subcalcic augite $W_{28–29}En_{66–68}Fs_{5–6}$. The composition of clinopyroxene depends on its stratigraphic location only in metagabbroids and grades from $W_{42–49}En_{43–47}Fs_{5–11}$ in gabbro of the Lower megarhythm

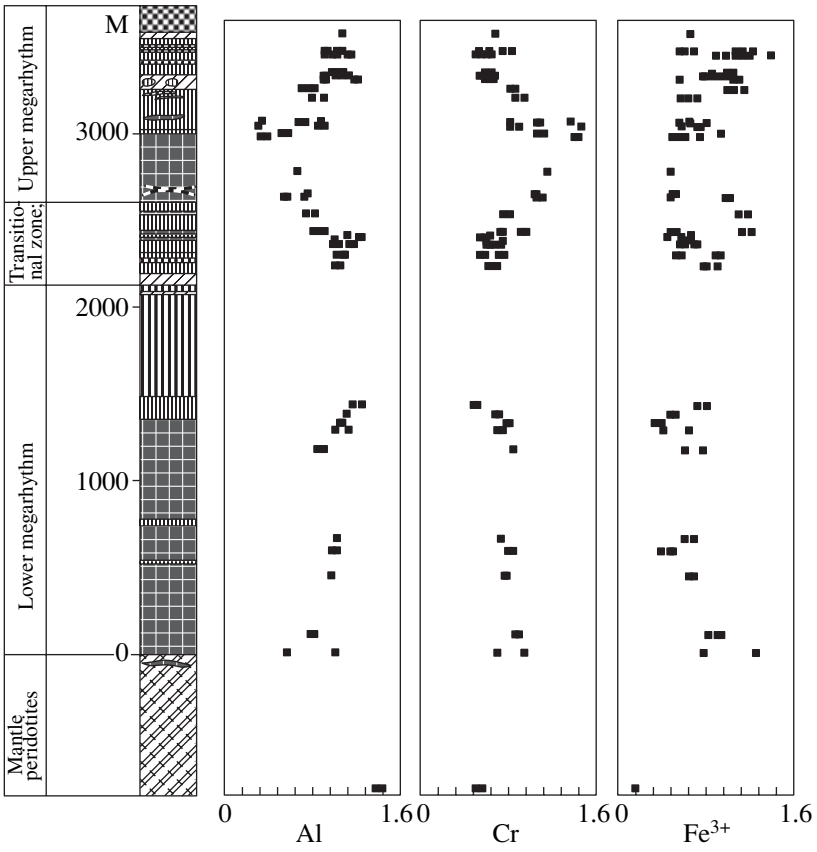


**Fig. 10.** Variation of spinel composition over the section.

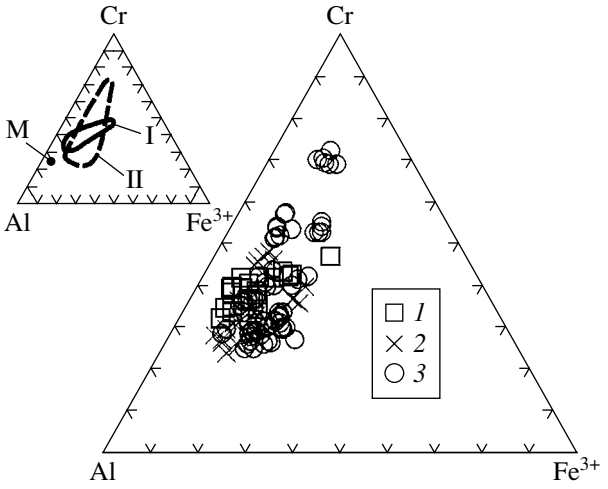


**Fig. 11.** Spinel compositions in a Cr–Al–$Fe^{3+}$ diagram. (*1*) Lower megarhythm, (*2*) Transitional zone, (*3*) Upper megarhythm. Small triangle shows fields of spinels from the Lower megarhythm (I), Upper megarhythm (II), and mantle spinel from the studied section (M).

to $W_{45–48}En_{38–47}Fs_{7–16}$ in the gabbronorite unit of the Upper megarhythm. Clinopyroxene in olivine gabbronorite veins in the dunite horizon of the Upper megarhythm is more magnesian ($W_{47–48}En_{44–45}Fs_{7–8}$) than that in gabbronorites from the sheet bodies occurring further upsection ($W_{42–48}En_{41–46}Fs_{10–15}$), where it is similar to clinopyroxene from the host cumulates.

**Orthopyroxene** in olivine gabbronorites of the Upper megarhythm corresponds to bronsite ($W_{1–2}En_{80–81}Fs_{18–19}$) and significantly differs from orthopyroxene from the mantle harzburgites ($W_1En_{90}Fs_9$). The mineral is ever more ferrous in the sheet gabbronorite bodies ($W_{1–2}En_{69–74}Fs_{25–30}$).

Compositions of all the pyroxenes analyzed in the Voikar layered complex are shown in Fig. 7.

**Plagioclase** is generally represented by anorthite over the whole section and becomes more sodic up to $An_{85}$ only in the uppermost gabbronorites (Figs. 8, 9).

**Chrome spinels.** The most interesting results were obtained for spinels (Figs. 10, 11). They show a negative correlation between Al and Cr contents. Unlike the silicate minerals of mantle peridotites, mantle spinels make a separate compositional group with the lowest Fe and Cr contents. Spinels from the Lower megarhythm also form a separate cluster; they are more chromian and evolve to more ferric compositions. Spinels from the Upper megarhythm are the most diverse and range from the lower chromian varieties mentioned above to minerals with the highest $Cr_2O_3$ contents at 41.8 wt % (in the lower part of the section). The compositional fields of spinels from the Lower and Upper megarhythms overlap. Spinels from the Transitional zone between megarhythms have intermediate compositions. Upsection, Al contents increase and Cr contents decrease in spinels (only slightly in the lower megarhythm and more significantly in the upper megarhythm), and reverse changes are observed only in the Transitional zone, i.e., Cr contents in spinel increase upsection.

## COMPARISON WITH THE OMAN OPHIOLITES

Variations of mineral compositions in the Voikar layered complex are basically similar to those in the layered gabbro in the typical ophiolites of Oman in the north of the Oman Mountains. Excluding the minerals of the marginal dunites which are more magnesian and compositionally closer to the upper mantle rocks of Oman, olivine and clinopyroxene of the Voikar massif show similar Mg/(Mg + Fe) variations to those in the layered gabbro in the Rustaq block [12] and in the north of the Oman Mountains [13]. As in the Voikar massif, gabbronorites and norites are the most abundant rocks in the north of the Oman Mountains [13–15]. Plagioclase compositions in the Voikar layered complex are generally close to those in the Oman Mountains; however, the former are more calcic than the dominant plagioclases in Oman ($An < 90$). The Cr/(Cr + Al) variations in spinels of the Voikar complex are smaller than those in the south of the Oman Mountains [16].

The Voikar layered complex and the layered gabbro of Oman show no significant enrichment of rocks in iron as a result of in-chamber crystal fractionation, as is the case in the Skaergaard-type continental layered intrusions [17]. As in the Oman ophiolites, the rocks of the Voikar layered complex show direct and reverse trends of Fe/(Fe + Mg) variations in mafic minerals and Cr/(Cr + Al) in spinels (Figs. 5, 6, 10). The direct and reverse variations in both ophiolite associations are similar in stratigraphic location and compositional ranges. These factors indicate that the structure of the Voikar layered complex is not unique and is typical of the ophiolite associations.

## DISCUSSION

**Evolution of magmatic processes.** Based on the data obtained, we believe that the Voikar ophiolite association was originated by the crystallization of a periodically replenished open magmatic system in tectonically dynamic conditions. The lack of significant enrichment of olivines and pyroxenes in iron over the 4- to 5-km section of the complex suggests an open magmatic system, where fractional crystallization, magma eruption, and the ascent of new magma portions from the mantle were approximately balanced. The Sm–Nd isotopic studies in the rocks of the Voikar layered complex indicate a MORB-type magma source. According to mineral assemblages, the initial magmas corresponded to tholeiitic picrobasalts.

This magmatic system had a prolonged and complex evolution during at least two stages expressed in the formation of two megarhythms. The evolution of

both megarhythms began from the *Ol–CrSp* cumulates, which gradually passed (through the intercalation zone) to gabbroids. The Layered complex is similar in many respects to the continental layered intrusions, but the occurrence of the specific Transitional zone with reverse evolution from mafic to ultramafic rocks makes them distinct.

The moderately depleted upper mantle (probably, the ultrabasic rocks of the underlying mantle complex) was a magma source for the rocks of the Lower megarhythm. The relatively high Al content in chrome spinel and the absence of orthopyroxene in the rocks indicate that the magmas were derived from slightly depleted mantle domains at a relatively low melting degree. The gradual transition from dunites to gabbroids was probably related to the accumulation of residual magma resulting from crystal fractionation in a magma chamber.

Gradual changes from the slightly depleted to depleted mantle sources are exhibited only in the transitional zone, where Cr content in *CrSp* increases upsection and rare *Opx* grains appear. These factors probably indicate that the intensity of mantle convection and the partial melting degree have increased since that time.

The upper megarhythm indicates a new stage in the spreading zone evolution. Like the Lower megarhythm, dense picrobasaltic magma began to enter the magma chamber. However, according to the evolution of the *CrSp* composition upsection in the dunite horizon, the melts were primarily derived from the depleted mantle domains and, then, from the less depleted mantle material. These factors probably indicate the reactivation of mantle convection.

The occurrence of *Opx* in the rocks is also consistent with a more depleted mantle magma source. However, a principally new component appeared in the magma. Sharma *et al.* [2] demonstrated that one of the samples from the mantle section with the highest $f_{Sm/Nd}$ and $\varepsilon_{Nd}(0)$ values does not fall on the Sm–Nd mantle evolution line, whereas three other harzburgite samples are plotted on this line together with samples of rocks from the layered complex and the parallel dike complex. It is suggested that such an unusual harzburgite indicates the contribution of an old depleted mantle material, which could be tectonically involved through subduction into the new less depleted mantle. These rocks were intruded by basaltic melts that had ascended from a nondepleted source.

As was shown later, the Re–Os isotopic systematics in the upper part of the crustal section of the Voikar massif (*Ol* clinopyroxenite from the transitional zone, *Ol* gabbronorite from the upper megarhythm, and diabases from the parallel dike complex) shows one–two orders of magnitude lower Os contents than the rocks of the mantle section of the Voikar massif [1], and the $^{187}Os/^{188}Os$ ratios in the former are significantly higher than in the mantle rocks (up to 6.5 and 7.1 in the rocks of the layered complex and two times as high as in diabases).

**The tectonic setting and dynamics of the Voikar spreading center.** As follows from the petrological data and the close association of the Voikar ophiolites with island-arc complexes, these ophiolites represented fragments of the lithosphere of a back-arc sea [3]. This suggestion is supported by recent findings of boninitic rocks in the dike complex of the Voikar ophiolites [18]. The data above clarify the nature of deep-seated processes beneath a back-arc sea. Its evolution began with the upwelling of an asthenospheric plume composed of slightly depleted ultrabasic material. Separation of picrobasaltic magma began at a depth greater than 50–60 km under conditions of garnet lherzolite stability. However, according to the cumulative spinel compositions that are close to *CrSp* of the mantle part of the section, the most extensive melting occurred at lower depths under conditions of spinel lherzolite stability. The cooler portion of the plume (its head) is located above the area of magma generation, as is the case in continental rift zones [19].

According to the available geological data (see above) a magma chamber was formed directly on this relatively cool surface of the plume head and served to accumulate the newly formed magmas. These magmas crystallized to form the lower crust of the back-arc basin. This mechanism generally corresponds to underplating, i.e., the intrusion of mantle magmas along the crust–mantle boundary, and is one of the most important mechanisms of the continental lower crust formation [20].

**Structural–metamorphic transformations of ophiolitic rocks.** The following three types of rock alteration are typical of the Voikar association: (1) high-temperature blastic mylonitization, (2) appearance of metasomatic clinopyroxenite veins (second-type clinopyroxenites distinguished above), and (3) low-temperature shearing.

It is known [21] that high-temperature blastic mylonitization occurs in ophiolite associations only in mantle ultrabasic rocks and rocks of the layered complex (lower crust), which is expressed in the dominant ductile deformations. Upsection in the layered complex, these deformations grade to low-temperature shearing with brittle deformations having a dominant role and being particularly characteristic of the uppermost part of the layered complex abundant in massive gabbronorites and of the upper crustal rocks (pillow-lavas and parallel dike complex).

Voikar is not a unique massif. Shcherbakov [22] demonstrated that the complex folded structure of the mantle ultrabasic rocks originated during two stages of ductile deformation. Metamorphic banding and isoclinal folds were formed in harzburgites during the first-stage deformations expressed in the plane-parallel viscous plastic flow at a high temperature (~1200°C). The larger folds and the less strained folding structures were

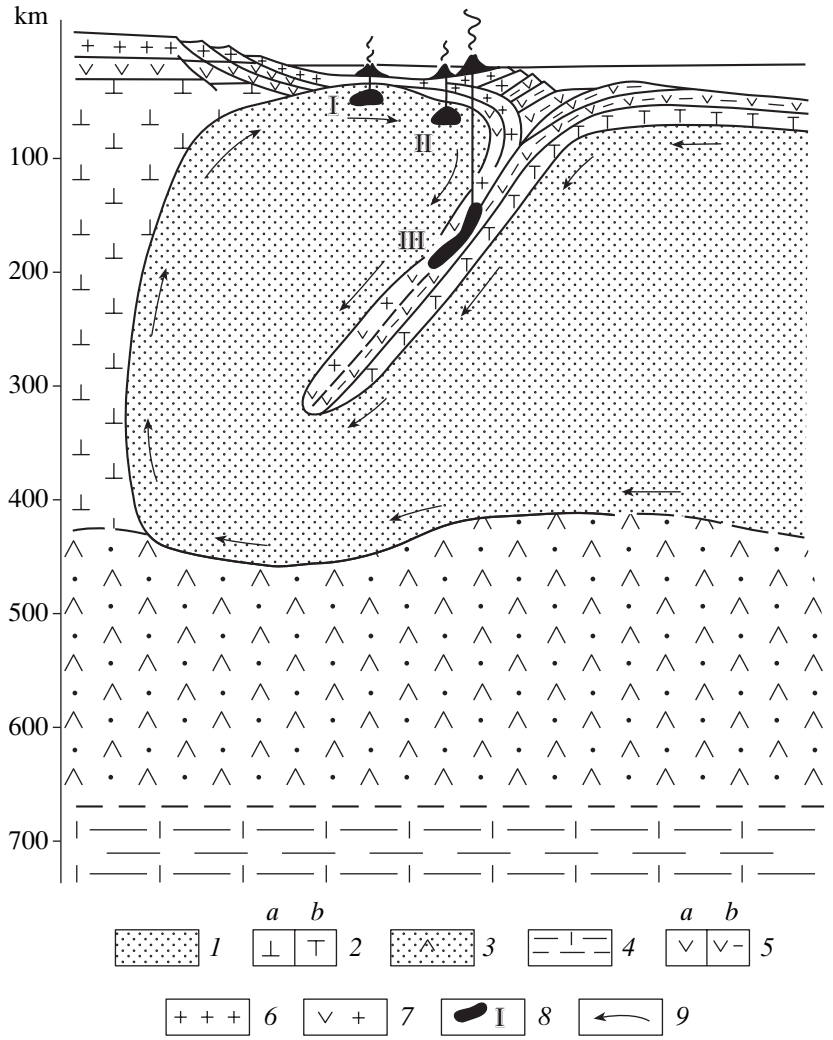


**Fig. 12.** Scheme illustrating the earlier stages of the back-arc spreading. (*1*) Asthenosphere; (*2*) upper mantle: *a*, continental segment and *b*, cool material of the superplume roof; (*3*) middle (transitional) mantle; (*4*) mantle below the discontinuity at 650–670 km; (*5*) "basaltic layer": *a*, continental and *b*, oceanic; (*6*) "granitic" layer; (*7*) tectonically mixed materials of the "basaltic" and "granitic" layers, (*8*) mantle domains generating magmas of different compositions: (I) tholeiitic, (II) boninitic, and (III) calc-alkaline; (*9*) direction of convection.

related to the plane-parallel shear plastic flow and originated during the second-stage deformations at lower temperatures (1000–700°C). The second-stage deformations in the rocks of the mantle complex were accompanied by the synkinematic formation of the layered ophiolite complex related to a combined effect of plastic flow, basaltic magma intrusion, and high-temperature metasomatism. According to Shcherbakov [22], spatial relationships and regularities in the orientation of deformation textures in the rocks of the layered complex indicate that these textures are related to a single phase of plastic deformations defined by harzburgites slipping relative to gabbroids.

Therefore, we could suggest that the first stage of deformations in mantle ultrabasic rocks was related to the mantle plume upwelling, and the second stage, to the spreading of the plume head beneath the spreading center. The hot mantle rocks of the plume head and solidified cumulates in the lower part of the crystallizing magma chamber were involved in a tectonic flow. These processes resulted in the high-temperature shearing of the newly formed rocks of the layered complex. Some of these high-temperature deformations could be related to a later shear stress, which accompanied the imbrication of heated mantle and lower crustal rocks during the closure of the back-arc basin (see below). These processes could have initiated a high-temperature reaction between olivine and plagioclase in some blastomylonitized gabbroids, which indicates a stress-related overpressure of up to 6–8 kbar (see above). However, such reaction structures are normally absent, thus indicating a lower lithostatic pressure. The traces of high-temperature shearing are absent in the upper

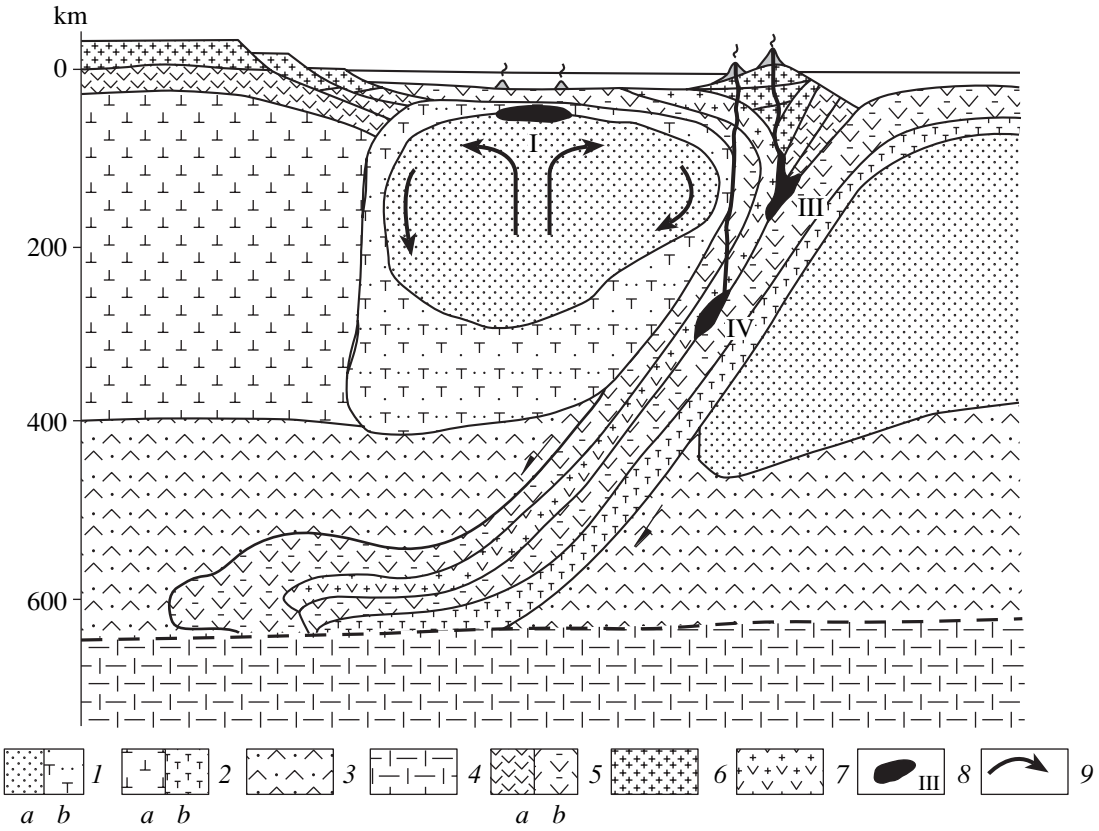


**Fig. 13.** Scheme illustrating the later stages of the back-arc spreading. (*1*) Asthenosphere: *a*, paltially melted and *b*, completely solidified; (*2*) upper mantle: *a*, ancient continental segments and *b*, cool material of the superplume roof; (*3*) middle (transitional) mantle; (*4*) mantle below the discontinuity at 650–670 km; (*5*) "basaltic layer": *a*, continental and *b*, oceanic; (*6*) "granitic" layer; (*7*) tectonically mixed materials of the "basaltic" and "granitic" layers, (*8*) mantle domains generating magmas of different compositions: (I) tholeiitic, (III) calc-alkaline, and (IV) K moderately alkaline (shoshonitic–latitic); (*9*) direction of convection.

crustal rocks (parallel dike complex) dominated by brittle deformations.

The high-temperature metasomatic clinopyroxenites were found only in the rocks of the Upper megarhythm. Their origin was probably related to fluids derived from the subduction zone and filtrated through heated rocks. These rocks are absent in the Lower megarhythm, and, therefore, we can suggest that they were sufficiently cool not to be involved in such interactions. It follows that the heat conduction could not provide homogeneous heating of the entire mass of the newly formed rocks.

The low-temperature rock shearing under greenschist-facies conditions was accompanied by the serpentinization of ultrabasic rocks and occurred significantly later, in the course of obduction of the back-arc sea lithospheric fragments over the margin of the Russian craton.

**The implied mechanism of deep-seated processes beneath the back-arc basins exemplified by the Voikar ophiolites.** We suggest the following evolution of the region. At the first stage, the mantle plume resulted from the outside expansion of an oceanic superplume, separated from the marginal part of a lithospheric block, and began to pull it toward the ocean (Fig. 12). The associated mechanical deformations caused the formation of zones of descending flows, i.e., a subduction zone, involving old mantle and crustal materials from the back-arc space. As a result, a back-arc basin with an oceanic crust was formed there. The magmatic rocks of the Lower megarhythm probably correspond to this stage. At a certain moment, the propagating subduction zone cut off the roots of the plume. This event hampered the supply of fresh mantle material, and the same mantle domains were remelted, which resulted in their progressive depletion. We believe that the Transitional zone was formed at that time. Then, the plume could break through the megalith, and the supply of fresh material proceeded; at this stage, the material from the subducted plate could also have been involved in the melting. The Upper megarhythm was probably generated at that time. The continuous thickening of the megalith finally isolated the upper part of the plume from its mantle root and terminated the evolution of the back-arc basin. A large lens of hot plastic mantle originated there and gradually

solidified from the bottom upward due to convection (Fig. 13). The existing stress field defined by the continuous spreading of the oceanic superplume would have been able to cause strong deformations in the upper part of the lithosphere of the back-arc sea, faulting of the crust and uppermost mantle, closure of the back-arc basin, and the formation of a foldbelt with the associated obduction of lithospheric fragments over the continental margin.

Thus, the first stage of formation of the Layered complex in terms of geodynamics could be related to the initial opening of the back-arc basin, and the second stage, with the initiation and development of a subduction zone. These processes resulted in the final isolation of the back-arc mantle plume head, the termination of its evolution, the closure of the back-arc basin, and the formation of a foldbelt in that area.

## CONCLUSIONS

(1) The Voikar ophiolite association is composed of lithospheric fragments of a Late Devonian back-arc sea in the western periphery of the Uralian Ocean.

(2) The Layered complex of these ophiolites (the back-arc sea lower crust originating from intrusions of newly formed magmas along the crust–mantle boundary) represents a shallow magma chamber, where the magmas accumulated and crystallized. This chamber evolved in two main stages. The Lower megarhythm (first stage) was formed from magmas derived from the moderately depleted mantle domains, while the primary magmas for the Upper megarhythm (second stage) were generated in the more depleted mantle with the addition of old material (probably, from the subducted plate) and subduction-related melts. The mantle convection was highly intensive during megarhythm formation.

(3) The Transitional zone between the megarhythms has a reverse rock sequence (grading upsection from basic to ultrabasic rocks) and is characterized by an upsection evolution to more depleted sources. This zone probably originated during a temporary decrease in the intensity of mantle convection between the periods of megarhythm formation.

(4) The formation of the lower crust was accompanied by the spreading of the mantle plume head, which resulted in high-temperature shearing of mantle peridotites in the uppermost part of the plume and of the overlying newly formed hot cumulates. The low-temperature shearing was probably related to obduction.

(5) In terms of geodynamics, the first stage of formation of the Layered complex could be related to the initial opening of a back-arc basin, and the second stage, to the initiation and development of a subduction zone.

The authors are thankful to G.N. Savelieva for helpful comments and to J.E. Quick for his assistance in analytical studies.

## REFERENCES

1. Sharma, M., Hofmann, A.W., and Wasserburg, G.J., Melt Generation beneath Ocean Ridges: Re–Os Isotopic Evidence from the Polar Ural Ophiolite, *Abstr. Goldschmidt Conf.,* Toulouse, 1998, vol. 3, pp. 1375–1376.
2. Sharma, M., Wasserburg, G.J., Papanastassiou, D.A., *et al.*, High $^{143}Nd/^{144}Nd$ in Extremely Depleted Mantle Rocks, *Earth Planet. Sci. Lett.*, 1995, vol. 39, pp. 101–114.
3. Laz'ko, E.E., Ultrabasic Rocks of Ophiolitic Suite, in *Magmaticheskiye gornyye porody* (Igneous Rocks), vol. 5, *Ul'traosnovnye porody* (Ultrabasic Rocks), Laz'ko, E.E. and Sharkov, E.V., Eds., Moscow: Nauka, 1988, pp. 8–96.
4. Nicolas, A., Structures of Ophiolites and Dynamics of Oceanic Lithosphere, Boston: Kluwer Academic, 1989.
5. Detrick, R.S., Ridge Crest Magma Chambers: A Review from Marine Seismic Experiments at the East Pacific Rise, in *Ophiolite Genesis and Evolution of Oceanic Lithosphere*, Peters, T., Nicolas, A., and Coleman, R.J., Eds., Boston: Kluwer Academic, 1991, pp. 7–20.
6. Quick, J.E. and Delinger, R.P., Ductile Deformation and the Origin of Layered Gabbro in Ophiolites, *J. Geophys. Res.*, 1993, vol. 93, pp. 14 015–14 027.
7. Zonenshain, L.P., Kuz'min, M.L., and Natapolov, L.M., *Geology of the USSR: A Plate-Tectonic Synthesis,* Washington: AGU, 1990, vol. 21.
8. Puchkov, V.N., Modern Views on the Tectonics of the Urals, *Geotektonika,* 1997, no. 4, pp. 42–61.
9. Saveliyeva, G.N., *Gabbro-ul'trabazitovaya assotsiatsiya Ural'skikh ofiolitov i ikh analogov v sovremennoi okeanicheskoi kore* (The Gabbro–Ultrabasic Association of Uralian Ophiolites and Their Analogues in the Modern Oceanic Crust), Moscow: Nauka, 1987.
10. Saveliyev, A.A. and Saveliyeva, G.N., Ophiolites of the Voykar Massif (Polar Urals), in *Ophiolites of the Canadian Appalachians and Soviet Urals*, Newfoundland: Memorial Univ., 1979, vol. 8, pp. 127–140.
11. Green, D.H. and Hibberson, W.H., The Instability of Plagioclase in Peridotite at High Pressures, *Lithos*, 1970, vol. 5, pp. 209–222.
12. Browing, P., Cryptic Variation within the Cumulate Sequence of the Oman Ophiolite: Magma Chamber Depth and Petrological Implications, in *Ophiolites and Lithosphere*, Gass, I.G. *et al.*, Eds., *Geol. Soc. London Spec. Publ.*, 1984, vol. 13, pp. 71–82.
13. Smelling, J.D., Mixing Characteristics and Compositional Differences in Mantle-derived Melts beneath Spreading Axes: Evidence from Cyclically Layered Rocks in the Ophiolite of North Oman, *J. Geophys. Res.*, 1981, pp. 2645–2660.

14. Juteau, T., Beurrier, M., Dahl, R., and Nehlig, P., Segmentation at a Fossil Spreading Axis. The Plutonic Sequence of the Wadi Haymiliayah Area (Haylayn Block, Sumail Nappe, Oman), *Tectonophysics,* 1988, vol. 151, pp. 167–197.

15. Lippard, S.J., Shelton, A.W., and Gass, I.G., The Ophiolite of Northern Oman, *Mem. Geol. Soc. London*, 1986, vol. 11.

16. Pallister, J.S. and Hopson, C.A., Samail Ophiolite Plutonic Suite: Field Relations, Phase Variation and Layering, and a Model of a Spreading Ridge Magma Chamber, *J. Geophys. Res.*, 1981, vol. 86, pp. 2593–2644.

17. Wager, L. and Brown, G., *Layered Igneous Rocks*, Edinburgh: Oliver & Boyd, 1968. Translated under the title *Rassloennye izverzhennye porody*, Moscow: Mir, 1970.

18. Simonov, V.A., Kurenkov, S.A., and Stupakov, S.I., Boninite Series in the Polar Ural Paleospreading Complexes, *Dokl. Akad. Nauk,* 1998, vol. 361, no. 2, pp. 232–235.

19. Sharkov, E.V., Snyder, G.A., Taylor, L.A., *et al.*, Geochemical Peculiarities of the Asthenosphere beneath the Arabian Plate: Evidence from Mantle Xenoliths from Quaternary Tell-Danun Volcano, Syrian–Jordan Plateau, Southern Syria, *Geokhimiya*, 1996, no. 9, pp. 819–835.

20. Rudnick, R., Growing from Below, *Nature*, 1990, vol. 347, no. 6295, pp. 711–712.

21. Nicolas, A., Reuber, I., and Benn, K., A New Magma Chamber Model Based on Structural Studies of Oman Ophiolite, *Tectonophysics*, 1988, vol. 151, pp. 87–105.

22. Shcherbakov, S.A., Textural Evolution of Ultrabasic Rocks of the Voikar–Syn'ya Ophiolite Massif, Polar Urals, *Izv. Akad. Nauk SSSR, Ser. Geol.*, 1989, no. 2, pp. 50–61.